Focussing the view on Nature's water-splitting catalyst

Samir Zein[1,2], Leonid V. Kulik[3], Junko Yano[4], Jan Kern[5], Yulia Pushkar[4], Athina Zouni[5], Vittal K. Yachandra[4], Wolfgang Lubitz[1], Frank Neese[2] and Johannes Messinger[1,*]

[1]Max-Planck Institut für Bioanorganische Chemie, Stiftstrasse 34-36, 45470 Mülheim an der Ruhr, Germany

[2] Lehrstuhl für Theoretische Chemie, Institut für Physikalische und Theoretische Chemie, Universität Bonn, Wegelerstr. 12, 53115 Bonn, Germany

[3] Institute of Chemical Kinetics and Combustion, Novosibirsk, Russia

[4] Physical Biosciences Division, MS: 66-0200, Lawrence Berkeley National Laboratory, 1 Cyclotron Rd., Berkeley, CA 94720, USA

[5]Max-Volmer-Laboratorium, TU Berlin, Strasse des 17. Juni 135, D-10623 Berlin, Germany

*corresponding author: messinger@mpi-muelheim.mpg.de

Keywords: photosystem II, oxygen evolution, manganese cluster, EPR/ENDOR, EXAFS, density functional theory (DFT)

Short Titel: Nature's water splitting catalyst

Abstract

About 3 billion years ago Nature invented a catalyst that splits water with high efficiency into molecular oxygen and hydrogen equivalents (protons and electrons). This reaction is energetically driven by sun light and the active centre contains relatively cheap and abundant metals: manganese and calcium. This biological system therefore forms the paradigm for all man made attempts for direct solar fuel production and several studies are underway to determine the electronic and geometric structures of this catalyst. In this report we briefly summarize the problems and the current status of these efforts, and propose a DFT-based strategy for obtaining a reliable high resolution structure of this unique catalyst that includes both the inorganic core and the first ligand sphere.

Introduction

In nature water splitting is performed within a membrane bound pigment-protein complex known as photosystem II (PSII). Each PSII complex harvests sun light by an 'antenna' that consists of about 200 chlorophyll and several carotenoide molecules. Four specially bound chlorophylls and a pheophytin molecule perform the primary charge separation within the reaction centre that creates a potential of ~ + 1.3 V. Each charge separation leads to the oxidation of a metal-oxygen complex, and water is split once four oxidizing equivalents have been accumulated in this water oxidising complex (WOC). The different oxidation states of the WOC are generally referred to as S_i states (S_0, …, S_4), where the index denotes the number of stored oxidizing equivalents relative to the lowest oxidation state of the WOC during the catalytic cycle. For the energetics of this reaction sequence, coupling of electron and proton movements via the protein matrix appears to be of essential relevance (Hillier and Messinger, 2005; Renger and Holzwarth, 2005; McEvoy and Brudvig, 2006).

Several techniques have contributed to the current picture about the WOC. Historically the greatest impact with regard to the knowledge about the metal ion arrangement in the WOC had EXAFS spectroscopy (Yachandra et al., 1996; Yachandra, 2005), assisted by vital information from EPR and ^{55}Mn-ENDOR spectroscopy (Britt et al., 2000; Kulik et al., 2005), as well as from bioinorganic model chemistry (Mukhopadhyay et al., 2004). In contrast, the equally important information on the ligand sphere has been obtained mostly from site directed mutagenesis in combination with FTIR and EPR spectroscopy (Debus, 2005), and by X-ray crystallography (Ferreira et al., 2004; Loll et al., 2005).

Below we briefly summarize this development and propose a strategy for obtaining a reliable high resolution structure of the WOC that includes the metal core and the first ligand sphere.

The Mn_4O_xCa cluster of the WOC

The WOC is now known to comprise four manganese ions and one calcium ion that are connected via several μ-oxo bridges (Mn_4O_xCa complex). Solution EXAFS revealed already in the 1980's and 1990's the presence of 2-3 Mn-Mn distances at 2.7-2.8 Å and 1-2 Mn-Mn distance at 3.3-3-4 Å. On that basis a set of 11 possible structural motives (some are presented in Figure 1 a-e) was proposed by the Berkeley group (DeRose et al., 1994), from which the dimer of dimers model was discussed most prominently (Figure 1a) (Yachandra et al., 1996).

Mn K-edge EXAFS measurements of PSII samples are normally limited to a range just below the Fe K-edge because of the natural iron content of PSII samples and because the energy resolution of the Ge X-ray fluorescence detector is not high enough to fully discriminate between Mn and Fe X-ray fluorescence. This restricts the distance resolution to about 0.14 Å. Employing a crystal monochrometer recently allowed to extend the energy range well beyond the Fe K-edge, which improved distance resolution to 0.09 Å. This type of experiments demonstrate the presence of three short Mn-Mn distances in the range between 2.70 and 2.85 Å (Yano et al., 2005b).

It was noticed early on that the third FT-EXAFS peak contains another contribution that was best assigned to a Mn-Ca interaction at ~ 3.4 Å (Yachandra et al., 1993). Since this proposal was controversial, this was proven in many different ways by the Berkeley group: i) Mn-EXAFS in samples where Ca was replaced by the better back scatterer Sr (Sr-PSII) showed an increased third FT peak, while the 3rd peak decreased upon Ca-depletion (Latimer et al., 1995; Latimer et al., 1998), ii) Sr-EXAFS in Sr-PSII samples revealed 2-3 Sr-Mn interactions that disappeared after NH_2OH treatment (Cinco et al., 1998; Cinco et al., 2004), and iii) Ca-EXAFS on samples from which all unspecific Ca was removed also alloed detection of the Ca-Mn interactions (Cinco et al., 2002).

Two anions, namely Cl^- and bicarbonate (BC), have been proposed to be cofactors in the water splitting reaction of PSII. While there is compelling biochemical evidence for a functional role of Cl^- (van Gorkom and Yocum, 2005), it is controversial whether it is (in some S states) a direct ligand of the Mn_4O_xCa cluster. Binding of the Cl^- analogue azide within 5 Å of the Mn_4O_xCa cluster was demonstrated by ESEEM spectroscopy (Yu

et al., 2005). Similarly, extended EXAFS measurements show an extra peak that may be assigned to Cl^- (Pushkar et al., 2007). On the basis of EXAFS measurements on Br^- substituted samples it was recently suggested that Cl^- is not a direct ligand to the Mn_4 cluster in the S_1 state (Haumann et al., 2006). In contrast to Cl^-, no sound evidence exists for BC binding within the WOC, and it is also highly controversial what kind of role it may play during photosynthetic water oxidation (Klimov and Baranov, 2001; Stemler, 2002; Clausen et al., 2005; Hillier et al., 2006).

EXAFS on solution samples does not allow extracting the orientations of the Mn-Mn and Mn-Ca vectors. Such information is, however, vital for a further selection between possible models and for placing such models in the correct orientation within the crystal structure of PSII (see below). Therefore, EXAFS measurements were performed initially on one-dimensionally ordered PSII samples that were obtained by painting and partially drying of PSII membrane fragments (BBY) on plane substrates. This approach allowed for example to determine that the Mn-Ca(Sr) vector is close to the membrane normal, while that of the 3.3 Å Mn-Mn vector is close to the plane of the thylakoid membrane (Robblee et al., 2001). Once PSII single crystals of large enough dimensions (~ 0.3 x 0.3 x 0.9 mm) became available polarized EXAFS was performed on these three dimensionally ordered samples. This allowed reducing the number of possible geometries for the Mn_4 core to one, while still four different relative positions for Ca remained (Yano et al., 2006). Two of these currently most reliable models of the inorganic core of the WOC are presented in Figures 1g and 1h.

A different model for the Mn_4O_xCa cluster (see Figure 1f) was previously proposed on the basis of X-ray crystallography (Ferreira et al., 2004). However, this model is less reliable because of i) limited resolution (3.5 Å) and ii) severe radiation damage that was shown to occur during X-ray diffraction data collection (Yano et al., 2005a). This radiation damage not only reduces the Mn(III) and Mn(IV) ions of the intact WOC to Mn(II), but also severely alters the structure of the Mn_4O_xCa cluster (Yano et al., 2005a). However, already the first X-ray data of PSII (Zouni et al., 2001) indicated the relatively compact arrangement of the Mn ions, and the two latest studies show that the Ca is positioned between the Mn ions and the reaction centre of PSII (Ferreira et al., 2004; Loll et al., 2005).

All structures shown in Figure 1 refer to the S_1 and S_2 states, which have almost identical geometries. Interestingly, the structure of the cluster is changing dramatically upon the S_3 state formation (Liang et al., 2000; Haumann et al., 2005) and is also different in the S_0 state (Robblee et al., 2002; Haumann et al., 2005). This structural flexibility may be key to the catalytic activity of the WOC.

EPR measurements of the S_2 state were among the first to demonstrate the involvement of Mn in storing the oxidizing equivalents in the WOC (Dismukes and Siderer, 1981). In principle, the cw EPR multiline signals of the S_2 and S_0 states do contain all the information about the electronic and geometric structures of these states. In practice, however, it has proven impossible to extract any unique information because of the large number of undetermined fitting parameters. Significant progress was made on the basis of ^{55}Mn-ENDOR measurements on the S_2 state, which allow extracting reliable hyperfine interaction parameters. The analysis of these data strongly disfavoured the dimer of dimers model (Figure 1a), and instead preferred two others models of the initial EXAFS–derived set that were referred to as 'dangler' models (Figure 1b and 1c) (Peloquin et al., 2000). In the light of extra information from EXAFS and X-ray crystallography, subsequently the more connected dangler model d (Figure 1) was selected from the initial EXAFS derived set of structures (Britt et al., 2004). This model bares similarities to a structure suggested earlier by Kusunoki and coworkers (Hasegawa et al., 1999). In a separate effort the 'funnel' model (Figure 1e) was favoured based on EPR data (Carell et al., 2002).

Recently Q-band ^{55}Mn-ENDOR measurements were obtained from the S_0 and S_2 states of PSII (Kulik et al., 2005). A thorough analysis shows that the latest EXAFS derived structural models (Figure 1g, 1h) are fully consistent with the ^{55}Mn-ENDOR data (Kulik et al., submitted). Our preferred coupling schemes for the S_0 and S_2 states are shown in the left row of Figure 2. They are identical for model g(II) and h(III), because the two EXAFS models have the same Mn_4O_5 core.

^{55}Mn-ENDOR is, however, not a sharp knife, and valid solutions can, for example, also be found for the S_0 and S_2 states for the modified dangler (model d, Figure 1) and the crystallography derived model f (Figure 1). These solutions are also displayed

in Figure 2. Although the agreement between known structural changes between S_0 and S_2 and between the proposed structures and the calculated *J*-couplings is clearly less satisfying for models d and f (Figure 1) than for models g(II) and h(III), the former two can not be strictly excluded.

The ligands of the Mn_4O_xCa cluster in the WOC

EXAFS spectroscopy does not give any specific information on the ligands of the Mn_4O_xCa cluster. Detailed mutagenesis studies in combination with fluorescence, EPR and FTIR measurements revealed several possible ligands (Debus, 2005), many of which were found near the Mn_4O_xCa cluster in the recent X-ray diffraction (XRD) studies (Ferreira et al., 2004; Loll et al., 2005). However, some conflicts exist between these independent approaches (Debus, 2005) and also between the two latest crystal structures. Similarly, placing the polarized EXAFS derived models for the Mn_4O_xCa cluster into the XRD structures (Yano et al., 2006) results in unsatisfying metal-ligand distances, coordination numbers and geometries for all four possible models. This is shown for model h (Figure 1) in Figure 3. These discrepancies can be explained by i) the limited resolution of the X-ray structures and ii) the radiation damage occurring during the XRD measurements, which not only affects the cluster geometry, but likely also modifies the ligand positions. These factors also prevent the important localization of the substrate water binding sites.

A DFT based strategy for deriving a 'complete' model of the WOC

As summarized above, reliable information is now available about the positions of the four Mn ions in the WOC: on the basis of polarised single crystal EXAFS two very similar μ-oxo bridging motifs can be inferred, and only four specific options remain for the position of Ca (Yano et al., 2006). By contrast, several uncertainties remain for the important ligand environment and the bridging between Mn and Ca, resulting in a still

blurred view of the WOC. Since currently no significant progress is in sight for obtaining radiation damage free XRD structures of PSII, we decided to embark on a DFT based strategy for building a reliable model of the WOC that includes the Mn_4O_xCa cluster and its direct ligands. Previous DFT studies on the WOC have mostly concentrated on model f (McEvoy et al., 2005; Siegbahn and Lundberg, 2006; Sproviero et al., 2006, 2007) or on required mechanistic and structural features for O-O bond formation (Blomberg et al., 1997; Siegbahn and Crabtree, 1999; Siegbahn, 2000; Siegbahn and Blomberg, 2000; Lundberg et al., 2003, 2004; Lundberg and Siegbahn, 2005; Siegbahn, 2006).

In our approach towards a better 'focussed' view on this important catalyst we start from models of the Mn_4O_xCa cluster as determined by polarised EXAFS spectroscopy on PSII single crystals ((Yano et al., 2006); models g and h in Figure 1). Because we regard this information to be the most reliable available at present, we initially fix the metal positions. To these models we add various ligand environments that are consistent with information available from XRD, mutagenesis and FTIR spectroscopy. These ligands are pre-positioned by hand, and than computationally optimized as described below. After this first energy minimization, we release for the final geometry optimization also the metal positions. The correct structure should reveal itself by minimal structural changes during the final optimization step, and by good agreements between experimental spectroscopic parameters from EXAFS, XANES, EPR and ENDOR and those calculated by DFT-methods from the derived models.

Below we describe our initial efforts in this direction using a series of selected models.

Model construction

All models are built based on the structure of the Mn_4O_xCa cluster in the S_1/S_2 state as available from EXAFS studies (Yano et al., 2006). The positions of the four manganese atoms (A, B, C and D; see Figure 2), of Ca and of five oxygen atoms are available from the supplementary material of the above cited paper.

So far, only structures II (g in Fig. 1), IIa and III (h in Figure 1) of Yano et al. (Yano et al., 2006) were considered. Model I (Yano et al., 2006) appears less likely, since

the Mn-Ca vectors are not along the membrane normal. In this preliminary work we have focused on four models that are considered to be promising candidates for the actual structures of the S_1 and S_2 states of PSII. In order to reduce our models to a size that makes extended DFT studies feasible (~ 80 atoms, including the 5 metals), acetic acid anions have been considered to represent glutamate, aspartate and the alanine C-terminus of the D1 protein, and only the imidazole ring of the histidine amino acid was included in the models.

The starting structures of all models considered in this study have the following common features: D1-Asp170 is a monodentate ligand of MnA (for labelling of the Mn ions see Figure 1), D1-Glu333 is bridging between MnA and MnB, CP43-Glu354 is bridging MnB and MnC, D1-His332 ligates MnC, and D1-Glu189 is a bidentate ligand to calcium. Other protein ligands are placed model specific as explained below. Then, the coordination sphere of each manganese ion was completed (to six coordinate) with water molecules or hydroxyl ions, with the exception of model III-Cl, where one Cl^- is assumed to take the place of one water molecule at MnA (top rows in Figures 4 and 5).

In the starting geometry of model II (Fig. 4; top, left), D1-Asp342 is a monodentate ligand of MnC, and the C-terminus of D1-Ala344 is bridging between MnD and Ca. The main differences between models II and IIa (Fig. 4; top row) are the position of the calcium ion (as suggested by EXAFS), the replacement of the D1-Asp342 ligand at MnC by a water molecule, and that the C-terminus of D1-Ala344 is a bidentate ligand to MnD.

Models II (Fig. 4; top, left) and III (Fig. 5; top, left) differ mainly in the position of the μ_3-oxo bridge, which is pointing towards Ca in model II, while in model III the μ_3-oxo bridge is on the other side of the Mn trimer plane. This affects the way Ca may be bridged to Mn and also the positioning of other ligands such as CP43-Glu354. In the initial geometry of model III, the C-terminus of D1-Ala344 ligates in a bidentate fashion MnD, and D1-Asp342 is a monodentate ligand of MnC. For exploring the effects of possible chloride coordination to the Mn_4O_xCa cluster we replaced one of the water molecules ligating MnA in model III by Cl^- (model III-Cl; Fig. 5; top, right). One more

difference between models III and III-Cl is that in the latter D1-Asp342 is bridging MnC and MnD.

Based on proton release and electrochromic shift measurements the total charge of the WOC in the S_2 state is likely to be +1 (assuming that it is zero in the S_1 state) (Schlodder and Witt, 1999). Therefore protons have been added to the above residues in a way to obtain a total charge of the complex equal to +1. For this charge counting, three manganese atoms are assumed to be in oxidation state IV (d^3) and the fourth one to be in oxidation state III (d^4).

Calculations details

Geometry relaxations have been performed using the Gaussian 03 (Frisch et al., 2004) optimizer as implemented in the ORCA package (Neese, 2006b), with the BP86 (Perdew, 1986; Becke, 1988) functional and TZVP (Schäfer et al., 1994) basis set for all atoms. In the present work we have sidestepped the difficult problem of the correct spin-coupling of the Mn-ions by performing the calculations for a ferromagnetic spin alignment. While this will not be appropriate for property predictions, the effect on the optimized geometries should be very limited (Sigfridsson et al., 2001). For the analysis of the electronic structures of the relaxed geometries, single point calculations have been performed using the B3LYP (Becke, 1993b, a) functional and the TZVP basis set for all atoms. Specifically we obtained by this method the Löwdin charge (Szabo and Ostlund, 1989) and spin density distributions. Total energies were also calculated, but cannot be compared for the different models since they contain different sets of ligands. The obtained distribution of the oxidation states on the manganese centres was not imposed, but is a result of the calculations.

Results of the constrained optimization

As explained above the initial constrained optimization was performed for the S_2 state of the WOC with the metal positions fixed to the values determined by EXAFS

spectroscopy (Yano et al., 2006). The optimization of the positions of the ligand atoms of models II and IIa led to some changes in the coordination environment of the Mn ions as shown in the lower part of Figure 4. For model II the following changes are observed: 1) Migration of a proton from one of the water molecules ligated to MnA towards D1-Glu189. This change leaves a hydroxo ligand at MnA in the partially optimized structure. In addition, D1-Glu189 changes from being a bidentate ligand to Ca to being a monodentate one. 2) The position of CP43-Glu354 changes in a way that it no longer bridges MnB, MnC and MnD, but is almost a monodentate ligand of MnB, with a much larger distance (2.4 Å) to MnD. This leaves MnC, and practically also MnD in a 5 coordinate geometry.

The latter change occurs in a similar fashion also during the constrained optimization of model IIa, only that the ligation of CP43-Glu354 to MnD remains intact (Fig. 4; bottom, right). However, for model IIa the C-terminus of D1-Ala344 changes from being a bidentate ligand to being a monodentate ligand of MnD, which is consistent with conclusions from FTIR spectroscopy (Chu et al., 2004). Therefore, MnD is again in a 5-coordinate ligand environment after constrained geometry optimization.

During the constrained optimization of model III the C-terminus of D1-Ala344 changes like for model IIa from being a bidentate to being a monodentate ligand of a 5-coordinate MnD (Fig.5; bottom, left). In contrast, ligation of CP43-Glu354 is stable for models III and III-Cl and MnC remains 6-coordinate. Model III shows the formation of an H-bond between the water molecule bridging MnD and Ca and one of the two μ-oxo bridges between MnA and MnB, which brings these two oxygens into a suitable geometry (O-O distance of 2.48 Å) for later O-O bond formation. Interestingly, in case of Cl^- binding to MnA (Model III-Cl in Fig. 5; right side) the proton is transferred from this hydrogen bonded water molecule to the μ-oxo bridge, which elongates the MnA-O and MnB-O distances.

The constrained optimizations of both II and IIa (S_2 state) converged toward wave functions characterized by the oxidation states Mn_{ABCD}(IV,IV,IV,III) on manganese A, B, C, D, respectively (Table 1). The partial geometry relaxations of models III and III-Cl lead to different charge and spin density distributions relatively to each other. Model III

also presents the oxidation states Mn_{ABCD}(IV,IV,IV,III), while for III-Cl the oxidation states distribution is Mn_{ABCD}(III,IV,IV,IV). The preference for finding Mn(III) in position D is very likely the consequence of MnD being 5-coordinate in models II, IIa and III after the constrained geometry optimization. This may explain the difference to the oxidation state assignment presented in the coupling scheme of model II/III in Figure 2 (S_2 state). It is likely that with a modified ligand environment a different assignment is obtained. In case of model III-Cl for example, MnA attains oxidation state III and MnD is found in a 6-coordinate environment.

	Charge distribution					Spin density distribution			
	A	B	C	D	Ca	A	B	C	D
II	0.66	0.64	0.66	0.78	1.52	2.95	2.97	2.96	**3.85**
IIa	0.64	0.64	0.63	0.82	1.53	2.87	2.94	2.91	**3.85**
III	0.65	0.63	0.66	0.78	1.49	2.87	2.98	2.96	**3.84**
III-Cl	0.61	0.62	0.62	0.71	1.49	**3.86**	2.94	2.89	3.00

Table 1: Löwdin (Szabo and Ostlund, 1989) population analysis of the manganese cluster after partial optimization as obtained from B3LYP/TZVP single point calculations. In general, partial charges of all metallic ions are much smaller than their relative formal charges due to the ligand-to-metal electron donation. The partial charge of calcium is only slightly reduced revealing the more ionic nature of the Ca-ligand bonds. This can also be seen from the Ca-ligand distances that are on average 0.2 to 0.5 Å longer than Mn-ligand distances (pdb coordinates of the optimised structures are given in the supporting material). The spin density distributions show that about four unpaired electrons ($d^4 \rightarrow$ MnIII) are located on the Mn-D for models II, IIa, III and only three unpaired electrons can be found (on average) on each of the three other magnetic centres. However, for model III-Cl it is Mn-A which has the four unpaired electrons, instead.

Full optimization

The complete relaxation of the coordinates of the four considered models led to further structural changes, but the oxidation states distribution and the coordination scheme of all ligands remained the same as after the partial optimization, i.e. no further ligand migrations were observed (Figure 6).

Table 2 shows Mn-Mn and Mn-Ca distances before and after full optimization. In general the Ca-Mn distances changed more significantly during full optimization than the Mn-Mn distances. It is therefore remarkable that model IIa almost perfectly reproduces the experimentally determined values of the Mn-Ca distances. Model IIa gives also a fair

reproduction of the Mn-Mn distances, with the exception of the MnB-MnC distance being 0.1 Å too long and the MnB-MnD distance being 0.14 Å too short after full optimization. A difference of ~0.1 Å in the metal-metal distances is, however, likely within the precision limits of the present DFT-methodology. Better agreement with experimental values than to ~0.1 Å is not to be expected owing to the neglect of the protein environment, the chosen ferromagnetic spin alignment and the intrinsic error of the DFT methods. Another point that needs in future consideration is the possibility for protonations of μ-oxo bridges. Based on our experience of the past decade, (Neese, 2006a) metal-oxo bonds will be predicted with significantly higher precision (~0.02-0.03 Å) while the bonds to the more weakly bound terminal water ligands will typically be overestimated by 0.05-0.1 Å by the BP86/TZVP combination.

The MnA-MnB and MnC-MnD distances are well reproduced by all models (with the exception of the MnA-MnB distance in model III-Cl). In contrast, Model II is the only model that provides a good fit for the MnB-MnD (3.3 Å) distance. The MnB-MnC distance is for all fully optimized models 0.07 to 0.14 Å too long compared to the experimental data, and the closest match is found with models III and IIa.

		A-B	B-C	C-D	B-D	Ca-A	Ca-B	Ca-C	Ca-D
II	EXAFS	**2.72**	2.70	**2.80**	**3.29**	4.41	**3.75**	3.41	3.41
	DFT	**2.75**	2.84	**2.83**	**3.29**	3.68	**3.71**	4.08	3.78
IIa	EXAFS	**2.72**	**2.70**	**2.80**	3.29	**3.61**	**3.40**	**4.36**	**3.39**
	DFT	**2.73**	**2.80**	**2.80**	3.15	**3.52**	**3.43**	**4.27**	**3.42**
III	EXAFS	**2.72**	**2.72**	**2.80**	3.25	4.38	3.73	3.40	3.40
	DFT	**2.70**	**2.79**	**2.72**	3.50	3.98	3.87	3.71	3.53
III-Cl	EXAFS	2.72	2.72	**2.80**	3.25	**4.38**	**3.73**	3.40	**3.40**
	DFT	2.89	2.84	**2.77**	3.63	**4.29**	**3.70**	3.63	**3.39**

Table 2: Mn-Mn and Ca-Mn distances (Å) before (EXAFS) and after full geometry optimization (DFT) of the four considered models. The initial values are those determined by single crystal EXAFS spectroscopy (Yano et al., 2006). Distances that changed by 0.1 Å or less during full optimization are shown in bold. MnA-MnC and MnA-MnD distances are in all cases between 5 Å and 6 Å.

Discussion and Conclusions

The presented geometry optimized models represent a preliminary account of our efforts towards building a reliable model for the WOC. It cannot be expected that such an approach will easily lead to a unique answer concerning the detailed geometric structures of the various S_i states in the reaction cycle of PSII. We therefore do not compare these preliminary data in detail with data from the literature or our own proposals.

However, present calculations do provide i) some hints for directions that are worthwhile of further exploration, and ii) indicate that models II, IIa and III, which were proposed on the basis of polarized EXAFS on PSII single crystals, provide stable and chemically reasonable structures for the inorganic core of the WOC. They also reveal that relatively small differences in the ligand environments of models II, IIa and III, III-Cl have significant effects on the metal-metal distances and the spin-density distributions. This provides a basis for further optimizations, for which possibly also a slightly extended protein environment needs to be included, for example via the QM/MM method. This can be nicely seen by the effect that Cl^- binding to MnA has on the Mn-Ca distances, which are relatively remote from the Cl^- binding site (compare model III and III-Cl in Table 2). For the time being, model IIa and III appear to provide the best overall fit to the geometry, and small additional changes to the ligand sphere may lead to an even better agreement of all models with the available structural data for the S_1 (S_2) state.

Once a good agreement of all metal-metal distances is achieved, calculations of polarized EXAFS and XANES spectra and of EPR/ENDOR parameters will be performed to further test the reliability of such pre-selected structures. For electronic structure calculations the complex problem of the correct spin coupling in the cluster needs to be solved – a task that is far from being trivial and that requires the estimation of reasonable pair wise exchange couplings between the manganese ions in conjunction with the treatment of double exchange phenomena owing to the fact that the cluster is in a mixed valence state. These are the subjects of ongoing efforts in our laboratories.

Acknowledgements

JM and WL gratefully acknowledge the financial support by the DFG (Me 1629/2-4), the Max-Planck-Gesellschaft and the Solar-H program. SZ is the recipient of an Alexander von Humboldt fellowship. LK was supported by the President of the Russian Federation Grant for Young Scientists (MK-7440.2006.3) and the Russian Science Support Foundation. JK and AZ acknowledge support by SfB 498 (TP C7). VKY and JY acknowledge support from the NIH Grant GM 55302, and by the Director, Office of Science, Office of Basic Energy Sciences (OBES), Division of Chemical Sciences, Geosciences, and Biosciences of the Department of Energy (DOE) under Contract DE-AC02-05CH11231. Synchrotron facilities were provided by the Stanford Synchrotron Radiation Laboratory (SSRL), the Advanced Light Source (ALS), and the Advanced Photon Source (APS) operated by DOE OBES. The SSRL Biomedical Technology program is supported by NIH, the National Center for Research Resources (NCRR), and the DOE Office of Biological and Environmental Research, and BioCAT at APS is supported by NCRR.

References

Becke, A. D. 1988 Density-functional exchange-energy approximation with correct asymptotic-behavior. *Phys. Rev. A* **38**, 3098-3100.

Becke, A. D. 1993a A new mixing of Hartree-Fock and local density-functional theories. *J. Chem. Phys.* **98**, 1372-1377.

Becke, A. D. 1993b Density-functional thermochemistry. 3. The role of exact exchange. *J. Chem. Phys.* **98**, 5648-5652.

Blomberg, M. R. A., Siegbahn, P. E. M., Styring, S., Babcock, G. T., Åkermark, B. and Korall, P. 1997 A quantum chemical study of hydrogen abstraction from manganese coordinated water by a tyrosyl radical: a model for water oxidation in photosystem II. *J. Am. Chem. Soc.* **119**, 8285-8292.

Britt, R. D., Peloquin, J. M. and Campbell, K. A. 2000 Pulsed and parallel-polarization EPR characterization of the photosystem II oxygen evolving complex. *Annu. Rev. Biophys. Biomol. Struc.* **29**, 463-495.

Britt, R. D., Campbell, K. A., Peloquin, J. M., Gilchrist, M. L., Aznar, C. P., Dicus, M. M., Robblee, J. and Messinger, J. 2004 Recent pulsed EPR studies of the Photosystem II oxygen-evolving complex: implications as to water oxidation mechanisms. *Biochim. Biophys. Acta* **1655**, 158-171.

Carell, T. G., Tyryshkin, A. M. and Dismukes, G. C. 2002 An evaluation of structural models for the photosynthetic water oxidizing complex derived from spectroscopic and X-ray diffraction signatures. *J. Biol. Inorg. Chem.* **7**, 2-22.

Chu, H. A., Hillier, W. and Debus, R. J. 2004 Evidence that the C-terminus of the D1 polypeptide of photosystem II is ligated to the manganese ion that undergoes oxidation during the S_1 to S_2 transition: An isotope-edited FTIR study. *Biochemistry* **43**, 3152-3166.

Cinco, R. M., Robblee, J. H., Rompel, A., Fernandez, C., Yachandra, V. K., Sauer, K. and Klein, M. P. 1998 Strontium EXAFS reveals the proximity of calcium to the manganese cluster of oxygen evolving photosystem II. *J. Phys. Chem. B* **102**, 8248-8256.

Cinco, R. M., McFarlane Holman, K. L., Robblee, J. H., Yano, J., Pizarro, S. A., Bellacchio, E., Sauer, K. and Yachandra, V. K. 2002 Calcium EXAFS establishes the Mn-Ca cluster in the oxygen evolving complex of photosystem II. *Biochemistry* **41**, 12928-12933.

Cinco, R. M., Robblee, J. H., Messinger, J., Fernandez, C., Holman, K. L. M., Sauer, K. and Yachandra, V. K. 2004 Orientation of calcium in the Mn_4Ca cluster of the oxygen-

evolving complex determined using polarized strontium EXAFS of photosystem II membranes. *Biochemistry* **43**, 13271-13282.

Clausen, J., Beckmann, K., Junge, W. and Messinger, J. 2005 Evidence that bicarbonate is not the substrate in photosynthetic oxygen evolution. *Plant Physiol.* **139**, 1444-1450.

Debus, R. 2005 The catalytic manganese cluster: protein ligation. In *Photosystem II. The Light Driven Water:Plastiquinone Oxidoreductase* (Wydrzynski T and Satoh K (eds)), Advances in Photosynthesis Research Vol 22, pp. 261-284. Dordrecht: Springer.

DeRose, V. J., Mukerji, I., Latimer, M. J., Yachandra, V. K., Sauer, K. and Klein, M. P. 1994 Comparison of the manganese oxygen-evolving complex in photosystem II of spinach and *Synechococcus* sp. with multinuclear manganese model compounds by X-ray absorption spectroscopy. *J. Am. Chem. Soc.* **116**, 5239-5249.

Dismukes, G. C. and Siderer, Y. 1981 Intermediates of a polynuclear manganese cluster involved in photosynthetic oxidation of water. *Proc. Natl. Acad. Sci. USA* **78**, 274-278.

Ferreira, K. N., Iverson, T. M., Maghlaoui, K., Barber, J. and Iwata, S. 2004 Architecture of the photosynthetic oxygen-evolving center. *Science* **303**, 1831-1838.

Frisch, M. J., Trucks, G. W., Schlegel, H. B., Scuseria, G. E., Robb, M. A., Cheeseman, J. R., Montgomery, J., J. A., Vreven, T., Kudin, K. N., Burant, J. C., Millam, J. M., Iyengar, S. S., Tomasi, J., Barone, V., Mennucci, B., Cossi, M., Scalmani, G., Rega, N., Petersson, G. A., Nakatsuji, H., Hada, M., Ehara, M., Toyota, K., Fukuda, R., Hasegawa, J., Ishida, M., Nakajima, T., Honda, Y., Kitao, O., Nakai, H., Klene, M., Li, X., Knox, J. E., Hratchian, H. P., Cross, J. B., Bakken, V., Adamo, C., Jaramillo, J., Gomperts, R., Stratmann, R. E., Yazyev, O., Austin, A. J., Cammi, R., Pomelli, C., Ochterski, J. W., Ayala, P. Y., Morokuma, K., Voth, G. A., Salvador, P., Dannenberg, J. J., Zakrzewski, V. G., Dapprich, S., Daniels, A. D., Strain, M. C., Farkas, O., Malick, D. K., Rabuck, A. D., Raghavachari, K., Foresman, J. B., Ortiz, J. V., Cui, Q., Baboul, A. G., Clifford, S., Cioslowski, J., Stefanov, B. B., Liu, G., Liashenko, A., Piskorz, P., Komaromi, I., Martin, R. L., Fox, D. J., Keith, T., Al-Laham, M. A., Peng, C. Y., Nanayakkara, A., Challacombe, M., Gill, P. M. W., Johnson, B., Chen, W., Wong, M. W., Gonzalez, C. and Pople, J. A. 2004 *Gaussian 03 (http://www.gaussian.com/).* Wallingford CT Revision C.02

Hasegawa, K., Ono, T.-A., Inoue, Y. and Kusunoki, M. 1999 Spin-exhcange interactions in the S_2-state maganese tetramer in photosynthetic oxygen-evolving complex deduced from $g = 2$ multiline EPR signal. *Chem. Phys. Lett.* **300**, 9-19.

Haumann, M., Müller, C., Liebisch, P., Iuzzolino, L., Dittmer, J., Grabolle, M., Neisius, T., Meyer-Klaucke, W. and Dau, H. 2005 Structural and oxidation state changes of the photosystem II manganese complex in four transitions of the water oxidation cycle ($S_0 \rightarrow S_1$, $S_1 \rightarrow S_2$, $S_2 \rightarrow S_3$, and S_3,$S_4 \rightarrow S_0$) characterized by X-ray absorption spectroscopy at 20 K and room temperature. *Biochemistry* **44**, 1894-1908.

Haumann, M., Barra, M., Loja, P., Loscher, S., Krivanek, R., Grundmeier, A., Andreasson, L. E. and Dau, H. 2006 Bromide does not bind to the Mn_4Ca complex in its S_1 state in Cl^--depleted and Br^--reconstituted oxygen-evolving photosystem II: Evidence from X-ray absorption spectroscopy at the Br K-edge. *Biochemistry* **45**, 13101-13107.

Hillier, W. and Messinger, J. 2005 Mechanism of photosynthetic oxygen production. In *Photosystem II. The Light-Driven Water:Plastoquinone Oxidoredutase* (Wydrzynski T and Satoh K (eds)), Advances in Photosynthesis and Respiration Vol 22, pp. 567-608. Dordrecht: Springer.

Hillier, W., McConnell, I., Badger, M. R., Boussac, A., Klimov, V. V., Dismukes, G. C. and Wydrzynski, T. 2006 Quantitative assessment of intrinsic carbonic anhydrase activity and the capacity for bicarbonate oxidation in photosystem II. *Biochemistry* **45**, 2094-2102.

Klimov, V. V. and Baranov, S. V. 2001 Bicarbonate requirement for the water-oxidizing complex of photosystem II. *Biochim. Biophys. Acta* **1503**, 187-196.

Kulik, L. V., Epel, B., Lubitz, W. and Messinger, J. 2005 ^{55}Mn pulse ENDOR at 34 GHz of the S_0 and S_2 states of the oxygen-evolving complex in photosystem II. *J. Am. Chem. Soc.* **127**, 2392-2393.

Latimer, M. J., DeRose, V. J., Mukerji, I., Yachandra, V. K., Sauer, K. and Klein, M. P. 1995 Evidence for the proximity of calcium to the manganese cluster of photosystem II: determination by x-ray absorption spectroscopy. *Biochemistry* **34**, 10898-10909.

Latimer, M. J., DeRose, V. J., Yachandra, V. K., Sauer, K. and Klein, M. P. 1998 Structural effects of calcium depletion on the manganese cluster of photosystem II: determination by x-ray absorption spectroscopy. *J. Phys. Chem. B* **102**, 8257-8265.

Liang, W., Roelofs, T. A., Cinco, R. M., Rompel, A., Latimer, M. J., Yu, W. O., Sauer, K., Klein, M. P. and Yachandra, V. K. 2000 Structural change of the Mn cluster during the S_2 to S_3 state transition of the oxygen evolving complex of photosystem II. Does it reflect the onset of water/substrate oxidation? Determination by Mn x-ray absorption spectroscopy. *J. Am. Chem. Soc.* **122**, 3399-3412.

Loll, B., Kern, J., Saenger, W., Zouni, A. and Biesiadka, J. 2005 Towards complete cofactor arrangement in the 3.0 Å resolution structure of photosystem II. *Nature* **438**, 1040-1044.

Lundberg, M., Blomberg, M. R. A. and Siegbahn, P. E. M. 2003 Modeling water exchange on monomeric and dimeric Mn centers. *Theor.Chem. Acc.* **110**, 130-143.

Lundberg, M., Blomberg, M. R. A. and Siegbahn, P. E. M. 2004 Oxyl radical required for O-O bond formation in synthetic Mn-catalyst. *Inorg. Chem.* **43**, 264-274.

Lundberg, M. and Siegbahn, P. E. M. 2005 Minimum energy spin crossings for an O-O bond formation reaction. *Chem. Phys. Lett.* **401**, 347-351.

McEvoy, J. P., Gascon, J. A., Batista, V. S. and Brudvig, G. W. 2005 The mechanism of photosynthetic water splitting. *Photochem. Photobiol. Sci.* **4**, 940-949.

McEvoy, J. P. and Brudvig, G. W. 2006 Water-splitting chemistry of photosystem II. *Chem. Rev.* **106**, 4455-4483.

Mukhopadhyay, S., Mandal, S. K., Bhaduri, S. and Armstrong, W. H. 2004 Manganese clusters with relevance to photosystem II. *Chem. Rev.* **104**, 3981-4026.

Neese, F. 2006a A critical evaluation of DFT, including time-dependent DFT, applied to bioinorganic chemistry. *J. Biol. Inorg. Chem.* **11**, 702-711.

Neese, F. 2006b *ORCA - an ab initio, density functional and semiempirical program package.* University of Bonn, Germany Version 2.5.15

Peloquin, J. M., Campbell, K. A., Randall, D. W., Evanchik, M. A., Pecoraro, V. L., Armstrong, W. H. and Britt, R. D. 2000 ^{55}Mn ENDOR of the S_2-State multiline EPR signal of photosystem II: implications on the structure of the tetranuclear Mn cluster. *J. Am. Chem. Soc.* **122**, 10926-10942.

Perdew, J. P. 1986 Erratum: Density-functional approximation for the correlation energy of the inhomogeneous electron gas. *Physical Review B* **34**, 7406-7406.

Pushkar, Y., Yano, J., Glatzel, P., Messinger, J., Lewis, A., Sauer, K., Bergmann, U. and Yachandra, V. 2007 Structure and orientation of the Mn_4Ca cluster in plant photosystem II membranes studied by polarized range-extended x-ray absorption spectroscopy. *J. Biol. Chem.* **282**, 7198-7208.

Renger, G. and Holzwarth, A. R. 2005 Primary electron transfer. In *Photosystem II. The Light-Driven Water:Plastoquinone Oxidoreductase* (Wydrzynski TJ and Satoh K (eds)), Advances in Photosynthesis and Respiration Vol 22, pp. 139-175. Dordrecht: Springer.

Robblee, J. H., Cinco, R. M. and Yachandra, V. K. 2001 X-ray spectroscopy based structure of the Mn cluster and mechanism of photosynthetic oxygen evolution. *Biochim. Biophys. Acta* **1503**, 7-23.

Robblee, J. H., Messinger, J., Cinco, R. M., McFarlane, K. L., Fernandez, C., Pizarro, S. A., Sauer, K. and Yachandra, V. K. 2002 The Mn cluster in the S_0 State of the oxygen evolving complex of photosystem II studied by EXAFS spectroscopy: are there three di-μ-oxo-bridged Mn_2 moieties in the tetranuclear Mn complex? *J. Am. Chem. Soc.* **124**, 7459-7471.

Schäfer, A., Huber, C. and Ahlrichs, R. 1994 Fully optimized contracted Gaussian-basis sets of triple Zeta valence quality for atoms Li to Kr. *J. Chem. Phys.* **100**, 5829-5835.

Schlodder, E. and Witt, H. T. 1999 Stoichiometry of proton release from the catalytic center in photosynthetic water oxidation. *J. Biol. Chem.* **274**, 30387-30392.

Siegbahn, P. E. M. and Crabtree, R. H. 1999 Manganese oxyl radical intermediates and O-O bond formation in photosynthetic oxygen evolution and a proposed role for the calcium cofactor in photosystem II. *J. Am. Chem. Soc.* **121**, 117-127.

Siegbahn, P. E. M. 2000 Theoretical models for the oxygen radical mechanism of water oxidation and the water oxidizing complex of photosystem II. *Inorg. Chem.* **39**, 2923-2935.

Siegbahn, P. E. M. and Blomberg, M. R. A. 2000 Transition-metal systems in biochemistry studied by high-accuracy quantum chemical methods. *Chem. Rev.* **100**, 421-437.

Siegbahn, P. E. M. 2006 O-O bond formation in the S_4 state of the oxygen-evolving complex in photosystem II. *Chem. Eur. J.* **12**, 9217-9227.

Siegbahn, P. E. M. and Lundberg, M. 2006 Hydroxide instead of bicarbonate in the structure of the oxygen evolving complex. *J. Inorg. Biochem.* **100**, 1035-1040.

Sigfridsson, E., Olsson, M. H. M. and Ryde, U. 2001 Inner-sphere reorganization energy of iron-sulfur clusters studied with theoretical methods. *Inorg. Chem.* **40**, 2509-2519.

Sproviero, E. M., Gascon, J. A., McEvoy, J. P., Brudvig, G. W. and Batista, V. S. 2006 QM/MM models of the O_2-evolving complex of photosystem II. *J. Chem. Theo. Comp.* **2**, 1119-1134.

Sproviero, E. M., Gascon, J. A., McEvoy, J. P., Brudvig, G. W. and Batista, V. S. 2007 Quantum mechanics/molecular mechanics structural models of the oxygen-evolving complex of photosystem II. *Cur. Opin. Struc. Biol.* **17**, 173-180.

Stemler, A. J. 2002 The bicarbonate effect, oxygen evolution, and the shadow of Otto Warburg. *Photosynth. Res.* **73**, 177-183.

Szabo, A. and Ostlund, N. S. 1989 *Modern Quantum Chemistry. Introduction to advanced electronic structure theory.*, Mineola, NewYork: Dover Publications.

van Gorkom, H. J. and Yocum, C. F. 2005 The calcium and chloride cofactors. In *Photosystem II. The Light-Driven Water:Plastoquinone Oxidoreductase* (Wydrzynski T and Satoh K (eds)), Advances in Photosynthesis and Respiration Vol 22, pp. 307-328. Dordrecht: Springer.

Yachandra, V. K., DeRose, V. J., Latimer, M. J., Mukerji, I., Sauer, K. and Klein, M. P. 1993 Where plants make oxygen: a structural model for the photosynthetic oxygen evolving manganese cluster. *Science* **260**, 675-679.

Yachandra, V. K., Sauer, K. and Klein, M. P. 1996 Manganese cluster in photosynthesis: where plants oxidize water to dioxygen. *Chem. Rev.* **96**, 2927-2950.

Yachandra, V. K. 2005 The catalytic manganese cluster: organisation of the metal ions. In *Photosystem II. The Light-Driven Water:Plastoquinone Oxidoreductase* (Wydrzynski T and Satoh K (eds)), Advances in Photosynthesis and Respiration Vol 22, pp. 235-260. Dordrecht: Springer.

Yano, J., Kern, J., Irrgang, K. D., Latimer, M. J., Bergmann, U., Glatzel, P., Pushkar, Y., Biesiadka, J., Loll, B., Sauer, K., Messinger, J., Zouni, A. and Yachandra, V. K. 2005a X-ray damage to the Mn_4Ca complex in single crystals of photosystem II: a case study for metalloprotein crystallography. *Proc. Natl. Acad. Sci. USA* **102**, 12047-12052.

Yano, J., Pushkar, Y., Glatzel, P., Lewis, A., Sauer, K., Messinger, J., Bergmann, U. and Yachandra, V. K. 2005b High-resolution Mn EXAFS of the oxygen-evolving complex in photosystem II: structural implications for the Mn_4Ca cluster. *J. Am. Chem. Soc.* **127**, 14974-14975.

Yano, J., Kern, J., Sauer, K., Latimer, M. J., Pushkar, Y., Biesiadka, J., Loll, B., Saenger, W., Messinger, J., Zouni, A. and Yachandra, V. K. 2006 Where water is oxidized to dioxygen: structure of the photosynthetic Mn_4Ca cluster. *Science* **314**, 821-825.

Yu, H., Aznar, C. P., Xu, X. Z. and Britt, R. D. 2005 Evidence that azide occupies the chloride binding site near the manganese cluster in photosystem II. *Biochemistry* **44**, 12022-12029.

Zouni, A., Witt, H. T., Kern, J., Fromme, P., Krauß, N., Saenger, W. and Orth, P. 2001 Crystal structure of photosystem II from *Synechococcus elongatus* at 3.8 Å resolution. *Nature* **409**, 739-743.

Figure legends

Figure 1: Proposed models for the inorganic core of the water-oxidizing complex (WOC). Red balls symbolize manganese ions, blue balls oxygen bridges and the green ball the calcium ion. Dashed lines indicate that the bridging motif is unknown. Redrawn from (DeRose et al., 1994; Ferreira et al., 2004; Yano et al., 2006).

Figure 2: Proposed spin coupling schemes for the S_0 and S_2 states of the WOC that are consistent with Q-band ^{55}Mn-ENDOR data (Kulik et al., 2005). Red circles indicate the Mn ions, which are labelled A, B, C, D in the same way as in Figure 1. The Roman numbers in the circles give the formal oxidation states of the Mn ions. Calcium is not included in the spin coupling schemes since coupling between Mn ions via Ca is assumed to be negligible. The blue numbers give the *J*-couplings in cm^{-1} according to $H = -\Sigma J_{ik}(\mathbf{S}_i\mathbf{S}_k)$. The type of line represents the coupling strength: double line, strong antiferromagnetic coupling; single solid line, medium strength antiferromagnetic coupling; dashed lines, weak ferro- or antiferromagnetic coupling.

Figure 3: Ligand environment of model g(II) of Figure 1 as determined by placing this model into the 3.0 Å crystal structure (Loll et al., 2005; Yano et al., 2006). Panel A: electron density with model g(II). Panel B: Schematic view of the WOC. Blue dashed lines indicate that the displayed amino acids are too far away (> 3 Å) to be normally considered as ligands. Dashed black lines indicate metal ligand distances of less than 3 Å. Mn ions are indicated by red spheres, bridging oxygen's by gray spheres and Ca by a green sphere. For further details see (Yano et al., 2006).

Figure 4: Comparison of the initial structures (top) of models II and IIa with those obtained after constrained optimization (bottom). All indicated amino acids are from the reaction centre D1 protein of photosystem II, with the exception of Glu354, which is a side chain of the inner antenna CP43 protein of photosystem II. Alanine 344 is the C-terminus of the D1 protein and ligates via its terminal carboxy group. Manganese ions are indicated in purple, oxygen in red, hydrogen in white, calcium in green and carbon in black.

Figure 5: Comparison of the initial structures (top) of models III and III-Cl with those obtained after constrained optimization (bottom). All indicated amino acids are from the reaction centre D1 protein of photosystem II, with the exception of Glu354, which is a side chain of the inner antenna CP43 protein of photosystem II. Alanine 344 is the C-terminus of the D1 protein and ligates via its terminal carboxy group. Manganese ions are indicated in purple, oxygen in red, hydrogen in white, calcium in green, chloride in yellow, carbon in black, and nitrogen in blue.

Figure 6: molecular structures of II, IIa, III, and III-Cl models after constrained optimization (red) and after full optimization (blue). Manganese and calcium ions are represented by spheres. All hydrogen atoms are removed for clarity.

Figure 1

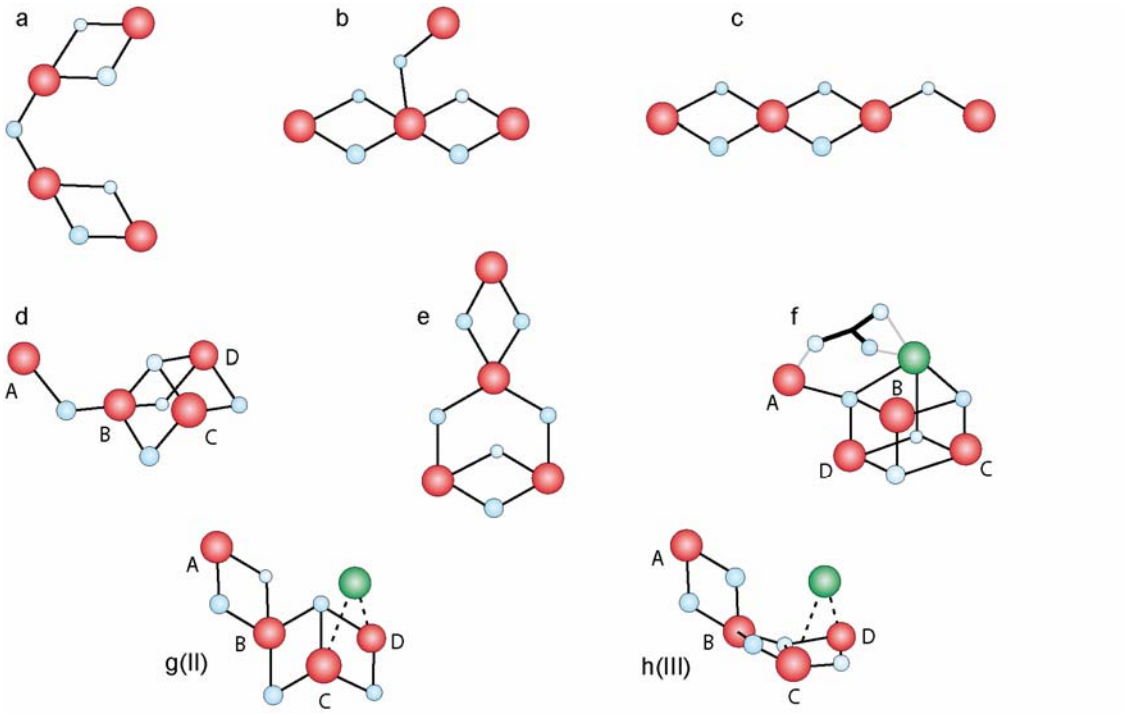

Figure 2

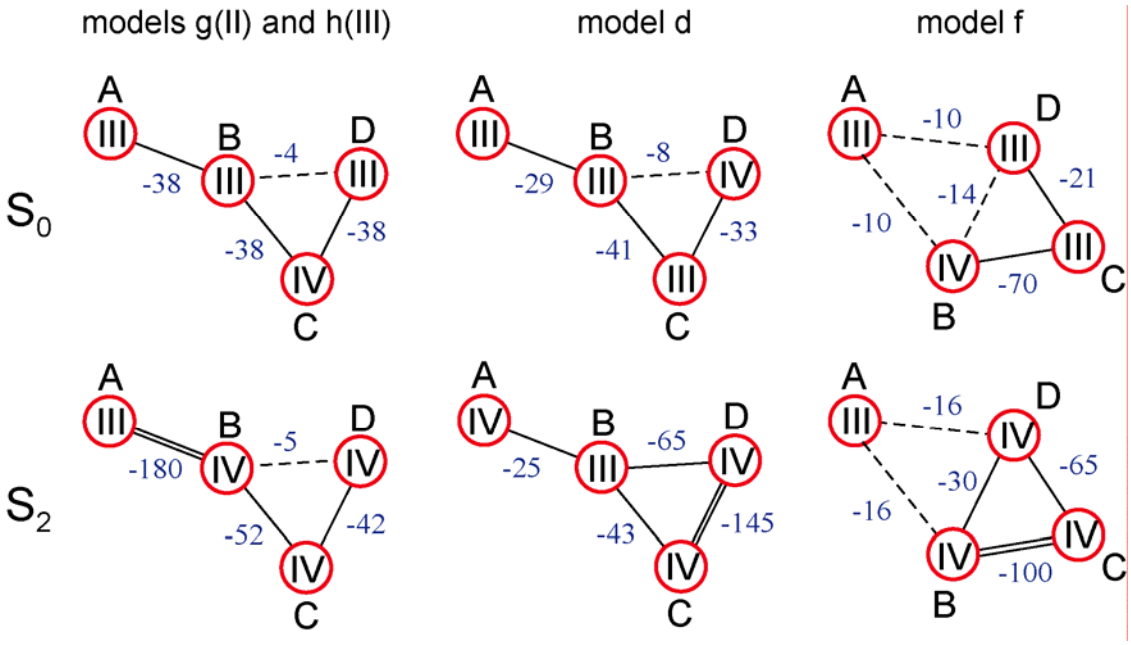
models g(II) and h(III)
model d
model f
S0
S2
A
B
C
D
III
IV
-4
-38
-38
-38
-8
-29
-41
-33
-10
-21
-14
-10
-70
-5
-180
-52
-42
-16
-65
-25
-43
-145
-30
-100

Figure 3

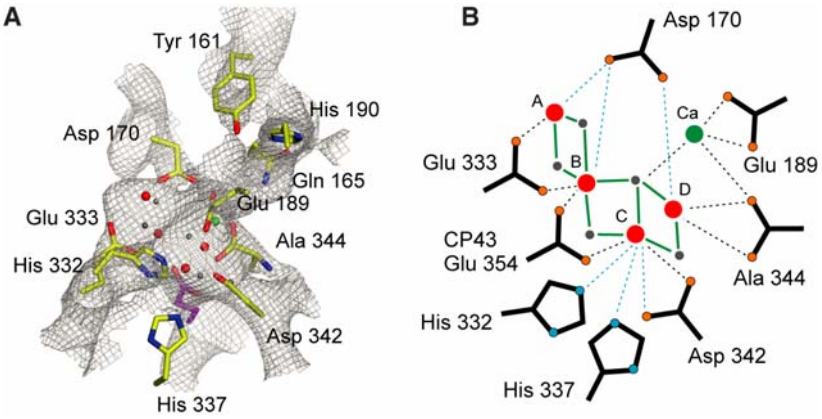
A
Tyr 161
His 190
Asp 170
Gln 165
Glu 189
Glu 333
Ala 344
His 332
Asp 342
His 337
B
Asp 170
A
Ca
Glu 333
B
Glu 189
D
C
CP43
Glu 354
Ala 344
His 332
Asp 342
His 337

Figure 4

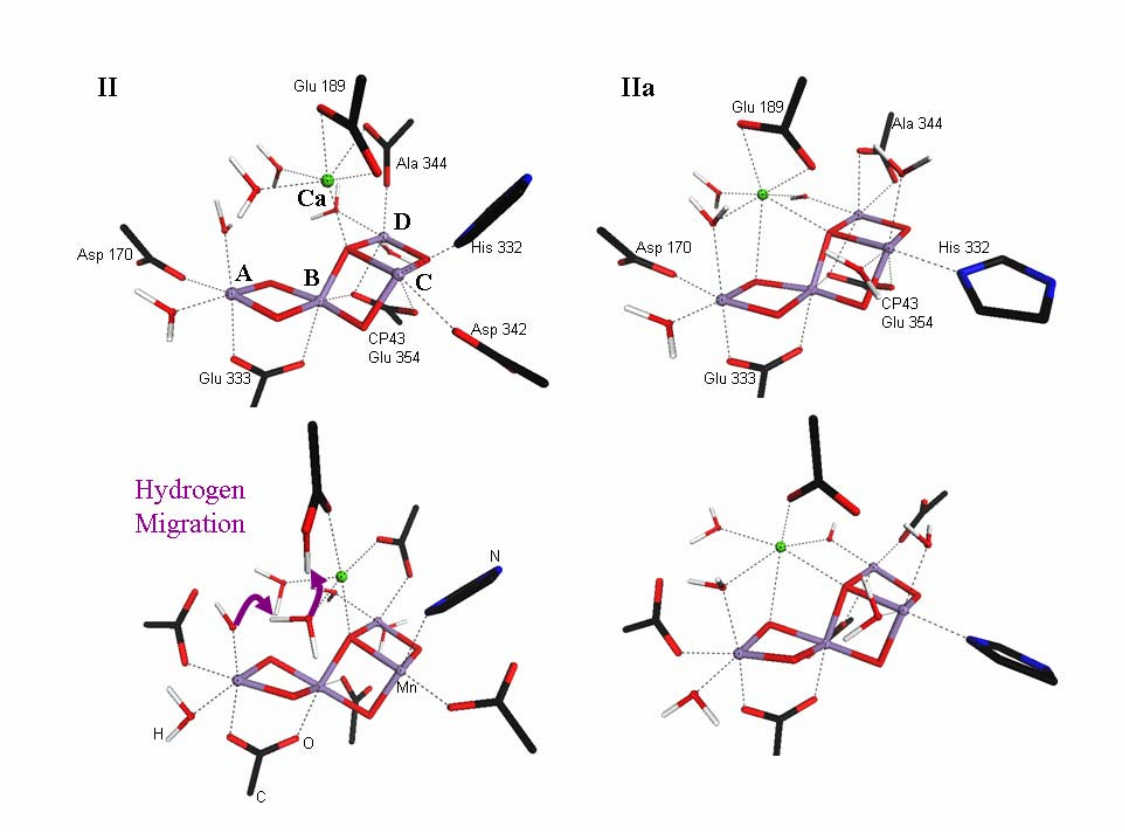
II
Glu 189
Ala 344
Ca
D
Asp 170
A
B
C
His 332
CP43
Glu 354
Asp 342
Glu 333
IIa
Glu 189
Ala 344
Asp 170
His 332
CP43
Glu 354
Glu 333
Hydrogen
Migration
N
Mn
H
O
C

Figure 5

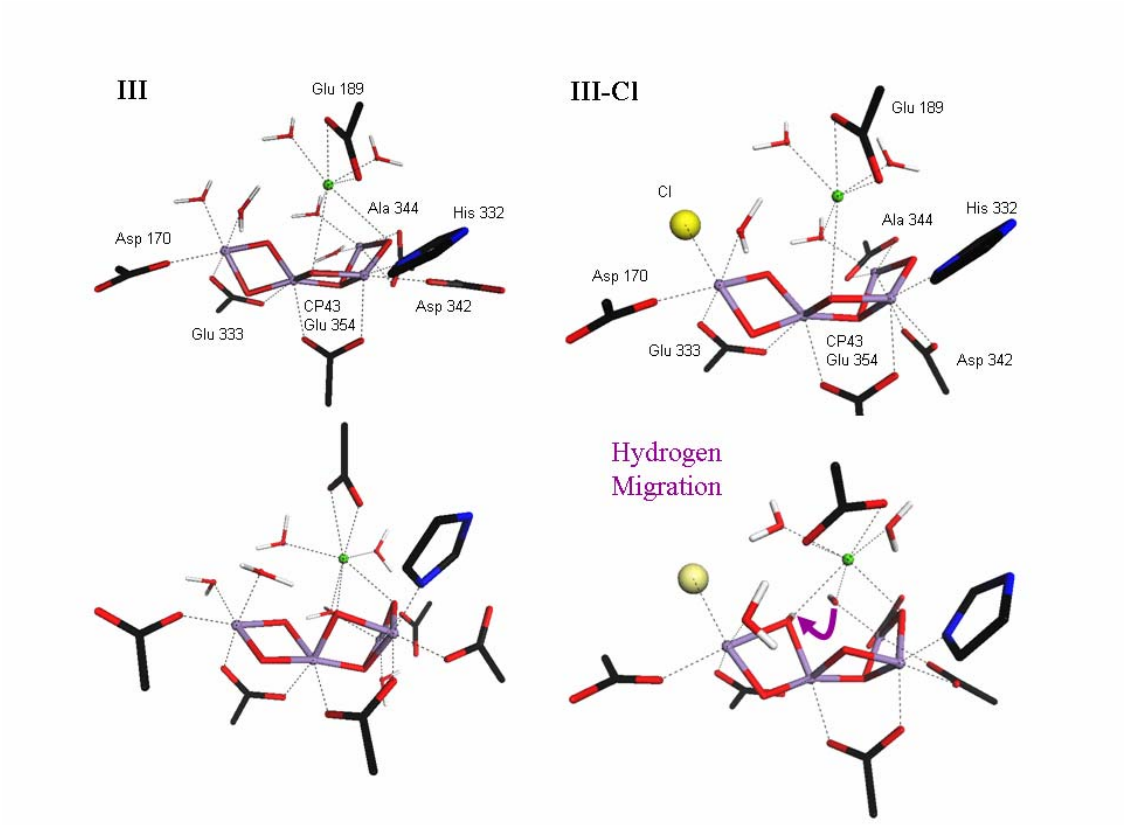
III
Glu 189
Ala 344
His 332
Asp 170
CP43
Glu 354
Asp 342
Glu 333
III-Cl
Glu 189
Cl
Ala 344
His 332
Asp 170
Glu 333
CP43
Glu 354
Asp 342
Hydrogen
Migration

Figure 6